# Interaction between acoustic cavitation bubbles and dispersed particles in a kHz-order-ultrasound-irradiated water

# Interaction between acoustic cavitation bubbles and dispersed particles in a kHz-order-ultrasound-irradiated water

**Yuki Mizushima[a], Yasuyuki Nagami[a], Yuta Nakamura[a] and Takayuki Saito[b*]**

[a]) Graduate school of Engineering, Shizuoka University, 3-5-1 Johoku, Naka-ku Hamamatsu, Shizuoka 432-8561, Japan

[b]) Graduate school of science and technology, Shizuoka University 3-5-1 Johoku, Naka-ku Hamamatsu, Shizuoka 432-8561, Japan

[*]) Corresponding Author, E-mail: ttsaito@ipc.shizuoka.ac.jp

Phone and Fax: +81 53 478 1601

**ABSTRACT:** In the past studies, MHz-order ultrasound has been frequently employed in the ultrasound separation techniques and the flocculation mechanism of particles due to the acoustic radiation force has been reported. The previous separation technique, however, is

applicable to particles with diameters similar to a wave length of the irradiated ultrasound or with smaller diameters than that. Hence, particles which are larger than μm-order in diameter are difficult to be manipulated with MHz-band ultrasound. In the present study, to clarify an unknown flocculation mechanism of the particles in an ultrapure water under kHz-band ultrasound irradiation, we quantitatively discussed an interaction between the particle motion and the acoustic cavitation bubble motion based on the experimental results. First, we successfully captured the particle motion and acoustic-cavitation-oriented bubble motion simultaneously by using a high-speed video camera. Second, we measured the distribution of the sound pressure in the water phase and discussed the relationship between that of the sound pressure and the motion of the particle and the acoustic cavitation bubble. Finally, we investigated the effects of the gravity force, the acoustic radiation force and the spatial heterogeneity of the pressure acting on the particle. By combining the results, we found out that an acoustic-cavitation-oriented bubble adhered to the particle and the particles moved toward the

pressure anti-nodes of the standing wave by the acoustic radiation force acting on the adhering acoustic-cavitation-oriented bubble.

**Keywords:** kHz-order ultrasound; Acoustic cavitation; Agglomeration; Bubble; Particle; Visualization.

## 1. INTRODUCTION

The ultrasound techniques are useful for solid-liquid separation. These methods, flocculating particles dispersed in the liquid phase, have practical advantages of simple apparatus, noncontact and chemical free operation. In the past studies, MHz-band ultrasound has been usually employed in this flocculation technique. King numerically derived an equation regarding acoustic radiation force acting on a small rigid sphere (King 1934). Nyborg reported that the particle flocculation is caused by the acoustic radiation force directly acting on the particles, and the particles are flocculated at a middle point of the wave length, i.e. pressure node or anti-node (Nyborg 1967). Kozuka

demonstrated selective manipulation based on an acoustic characteristic of the particles, and cell manipulation (Kozuka et al. 1997). Kozuka demonstrated 3D particle manipulation by using four sound sources and controlling the frequency (Kozuka 2005). Brotchie et al. found that the bubble size increased with increase in ultrasonic power and decreased with increase in ultrasonic frequency (Brotchie et al., 2009). Yamakoshi and Noguchi proposed a micro particle trapping system which was based on the opposite phases ultrasonic traveling waves; by driving two ultrasonic transducers placed side by side, the micro particles were trapped at the acoustic black line due to the spatially modulated acoustic radiation force (Yamakoshi and Noguchi, 1998). Woodside et al. experimentally determined a spatial distribution of ultrasonic forces, and presented a versatile method to measure the acoustic forces acting on dispersed particles as a function of their positions in the measurement area (Woodside et al., 1997). Woodside et al. also reported that the particles collect at the nodal planes of the standing-wave field due to the axial primary radiation force (Woodside et al., 1998). Takeuchi et al. proposed an ultrasonic technique to micro-manipulate very small particles in a liquid, utilizing the radiation pressure of a high-frequency ultrasound (Takeuchi et al., 1994). They reported the advantages of their technique were to efficiently generate

high-frequency ultrasonic waves in very small volume of the liquid containing small particles by using VHF-range leaky wave transducers. The particles were sufficiently smaller than the wavelength and were trapped at the pressure anti-nodes or nodes of the standing waves. This separation technique, however, is difficult to flocculate the particles which are larger than a wave length of the irradiated ultrasound. Therefore, particles larger than μm-order in diameter are difficult to be flocculated using MHz-band ultrasound. To overcome this problem, frequency of using ultrasound should be set lower. However, the studies on the kHz-band ultrasound almost were not reported previously. Leighton (1994) reported that the bubbles with sizes smaller than the resonant size moved up a pressure gradient toward pressure antinodes, and with those larger than resonant size moved down the gradient toward the node. Mitome (2001) reported that the particles moved toward pressure nodes in the standing wave when the density of the particle was larger than that of the liquid phase. Therefore, the mechanism of the particle flocculation is unknown yet. In order to find the positive application of kHz-band ultrasound and to achieve its practical use, it is essential to understand the flocculation mechanism. In our previous study, it was found out that the stationary position of the particle swarm corresponded with the gathering position of the acoustic

cavitation bubbles. Moreover, the particles were not flocculated when degassed water was employed. Then we reported that the acoustic cavitation bubbles significantly contribute to particles flocculation under kHz-band ultrasound irradiation (Nakamura et al. 2011).

In the present study, we investigated the particle flocculation under kHz-band ultrasound irradiation, which is very low compared with usual frequencies (MHz order) used in separation of small particles, in order to clarify the flocculation mechanism. Under kHz-band ultrasound irradiation, acoustic cavitation bubbles were generated in non-degassed water and not generated in degassed water. The particles were flocculated only in the non-degassed water and not flocculated in the degassed water. These differences are the mostly important in the present study. The unique aspect of this paper is to discuss both particles' and acoustic cavitation bubbles' motions, based on experimental results obtained under the kHz order ultrasound irradiation. Based on the results of the visualization of the particles' motions and the acoustic cavitation bubbles' motions and the measurement of sound pressure, we quantitatively discussed an interaction between the particle motion, the acoustic cavitation bubble motion and sound pressure distribution. Moreover, in order to understand the behaviour of the

particle swarm (flocculated particles), the influences of a particle diameter on the stationary position and diameter of the particle swarm were discussed in detail. As a consequence, the positions of the pressure anti-nodes of the standing waves were well corresponding with the positions at which the acoustic cavitation bubbles were gathered; furthermore the particles were also flocculated at the same positions. These phenomena indicated that the mechanism of particles flocculation under kHz-band ultrasound irradiation is different from the mechanism under MHz-band ultrasound irradiation.

## 2. EXPERIMENTAL SETUPS

### 2.1 Experiments for visualization of the particle motion and the acoustic cavitation bubble motion.

As shown in Fig. 1, the experimental setup employed in the present study mainly consists of an ultrasound driving system and a camera system. In the ultrasound driving system, which was all the same in the present study, a sine wave voltage signal generated by a function generator (a) (frequency: 20.3 kHz, output voltage: 1.00 V) was

supplied into a bolt clamped Langevin type transducer (c) (Honda Electronics, HEC-45254M) through a power amplifier (b). The ultrasound was irradiated upwardly-vertically from the bottom of an acrylic water vessel (d) (inner diameter: 50 mm, height: 120 mm). The vessel was filled with non-degassed ultrapure water (volume: 150 ml, temperature: 20°C) up to a depth of 76 mm. The cross-sectional center was defined as the origin of x axis (horizontal direction) and the vessel bottom was defined as the origin of z axis (vertical direction). In the camera system, in order to clarify the effects of acoustic cavitation bubble motion on the particle flocculation under kHz-band ultrasound irradiation, these motions were visualized simultaneously.

**Figure 1.** The schematic of the experimental setup.

In this experiment, the examined particle was approximately 300 μm in average diameter (polystyrene, density: 1.05 g/cm$^3$), the standard deviation of the diameter was 38.9 μm. While, the density of the water is 0.998 g/cm$^3$, and the particle concentration in the water was 0.67 g/L. The time-series images of the particle motion and the acoustic caviation bubble motion were captured by a high speed video camera (Photron,

FASTCAM SA1.1). The spatial resolution was 512 × 512 pixels (3.85 μm/pixel), and the frame rate was 20,000 fps. The interrogation area was positioned just under the stationary position of the particle swarm ($x$ was approximately 0 mm, $z$ was approximately 20 mm).

**2.2 Experiments of particle flocculation.**

The properties of the examined particles in this experiment are listed in Table 1. Four kinds of particles with different size were examined in each experiment. The vertical sectional images of the particle swarms in the vessel were captured by CCD camera (Hitachi, KP-F110). The spatial resolution was 1024 × 1024 pixels (64.5 μm/pixel), and the frame rate was 30 fps. In this experiment, the recording of the CCD camera started in 1 minute after the ultrasound irradiation.

**Table 1.** The properties of the particles.

**2.3 Measurement of the sound pressure.**

Sound pressure distribution in the vessel was measured by using a hydrophone

(Shinka Industry, SM1000). The frequency response range was 0 – 500 kHz, and the pressure measurement range was 0 – 896 kPa. The measurement accuracy was ±0.2 kPa. In this experiment, in order to measure the sound pressure in the vessel without cavitation bubble, we employed the degassed ultrapure water in which no acoustic cavitation bubbles were generated (Nakamura and Saito 2011). The measurement points were positioned at $z$ from 1 to 76 mm with an interval of 1 mm and at $x$ from 0 to 20 mm with an interval of 4 mm.

## 3. EXPERIMENTAL RESULTS AND DISCUSSIONS

### 3.1 The visualization result of the particle motion and the acoustic cavitation bubble motion.

The particle motion and the bubble motion which was thought to be induced by the acoustic cavitation bubbles were successfully captured by the high-speed video camera, simultaneously. Fig. 2 shows a set of typical time-series snapshots of a particle and bubbles adhering to the particle surface. From the visualization results, we confirmed that the largest bubble (acoustic-cavitation-oriented bubble), which iteratively expanded

and contracted, was adhering to the particle surface and leading the particle toward upper left. To quantitatively discuss the relationship between the particle motion and the acoustic-cavitation-oriented bubble motion, as shown in Fig. 3, we focused on the directions of these motions. First, in order to extract the contour of the particle and the adhering acoustic-cavitation-oriented bubbles from the raw image, the binarized image was processed by an appropriate binarization threshold. Second, the projected area of the particle and the acoustic-cavitation-oriented bubble (area A) was calculated by using image processing software (INSPECTOR Matrox Imaging software). By given diameter of the particle (i.e. average diameter of the particle), the area of the particle (area B) was calculated. Then, the area of the acoustic-cavitation-oriented bubble (area C) was calculated from the difference of area A and area B. The acoustic-cavitation-oriented bubble can be considered as a sphere since the area C was small, and the diameter of the acoustic-cavitation-oriented bubble was calculated. Third, based on the results of area B and area C, the particle and the acoustic-cavitation-oriented bubble were divided. Therefore, the gravity-centers of the particle and the acoustic-cavitation-oriented bubble were calculated. Fourth, the angle between the direction of the particle velocity vector and the direction of $x$ axis was defined as $\theta_v$ from the time-series results of the particle

gravity-centers. Fifth, the angle between the line connecting the center with the acoustic-cavitation-oriented bubble adhering position and the direction of $x$ axis was defined as $\theta_b$. Finally, the angular difference $\theta_d$ was calculated from $\theta_v$ and $\theta_b$. As shown in the Fig. 4, the histogram of the $\theta_d$ was calculated and the mode value of $\theta_d$ was 0. This result means that the largest bubble (the acoustic-cavitation-oriented bubble) adhering to the particle surface, and the particle moved toward almost the same direction, and indicates the particle flocculation was remarkably related to the acoustic cavitation bubbles.

**Figure 2.** Typical snapshots of a particle and the acoustic cavitation bubbles.

**Figure 3.** The definition of $\theta_v$ and $\theta_b$.

**Figure 4.** The histogram of $\theta_d$.

**3.2 The discussion of the influence of particle diameter on flocculation.**

In order to discuss the interaction between the acoustic cavitation bubble motion and the particle motion in more detail, we conducted an experiment of particle flocculation using four kinds of particle with different diameter (see Table 1). The particles were flocculated spherically and floating at approximately same position in the liquid phase. Typical results of the particle flocculation with 300 μm particles and 1000 μm particles in diameter are shown in Fig. 5(a) and 5(b). The initial particle concentration was 2 g/L. The stationary position of the particle swarm in Fig. 5(a) is higher than that in Fig. 5(b). The stationary positions depended on the particle diameter; i.e. the particle mass.

The relationship between the particle concentration and the particle swarm diameter against the particle diameter are shown in Fig. 6(a). The particle swarm diameter increased in proportion to the particle concentration. These results indicate the influence of particle diameter on the particle swarm diameter was small compared with the influence of particle concentration. Therefore, based on our experimental results, the flocculation technique using kHz-order ultrasound is applicable for flocculating the submillimeter polystyrene particles.

Fig. 6(b) shows the relationship between the particle concentration and the stationary position of the particle swarm against the particle diameter. There were two regions

located on *z* axis at from 15 to 30 mm and at 50 mm where the particle swarms were trapped. These positions were approximately same as the gathering positions of the acoustic cavitation bubbles. In order to confirm the gathering positions of the acoustic cavitation bubbles in the vessel, the authors conducted the visualization experiments to capture the acoustic cavitation bubbles by using Laser Tomography and to capture the sonoluminescence by using a CCD camera equipped with an Image Intensifier Unit (Hamamatsu Photonics K.K.). As shown in the Fig. 7, at 15 – 30 mm and about 50 mm of *z* axis, the gathering positions of the acoustic cavitation bubbles in the vessel are remarked by the red broken lines and correspond well with the positions where the particles flocculated. These results indicate the bubbles adhering to the particle lead the particle to the gathered positions of the acoustic cavitation bubbles. Moreover, the result that the stationary position was different depending on the particle diameter indicates the possible for the particle classification.

**Figure 5.** Particle swarms in the ultrapure water.

(a) Flocculated particles of 300 μm in average diameter.

(b) Flocculated Particles of 1000 μm in average diameter.

**Figure 6.** The results of a measurement of the particle swarm.

(a) Diameter of the particle swarm versus particle concentration.

(b) Particle concentration versus a stationary position of the particle swarm.

**Figure 7.** The visualization results of the acoustic cavitation bubbles captured by using Laser Tomography (left-side) and the sonoluminescence by using a CCD equipped with an Image Intensifier Unit (right-side).

### 3.3 The result of the measurement of sound pressure.

Fig. 8 shows the distribution of the sound pressure amplitude $P_s$ in the vessel. The distribution patterns near the vessel center ($x$ range of 0 – 8 mm) were different from those near the wall ($x$ range of 12 – 20 mm). The sound pressure amplitude near the center took a peak at $z$ of about 20 mm. While, the sound pressure amplitude near the wall took three peaks approximately at $z$ = 10, 40, 70 mm. The difference in the distribution patterns was considered to be caused by the interference between the incident wave and the reflected wave from the vessel wall. Because the ultrasound was

irradiated from the bottom to the top of the vessel in the present experimental setup, compared with the MHz band which always was employed in these kinds of studies, the sound directivity of kHz-band in the vertical direction was not very strong originally. In addition, 50 mm of the inner diameter of the vessel was comparable to the water level of 76 mm (i.e. wave length of 20.3 kHz ultrasound in water); the effects of the reflected wave from the vessel wall were stronger than that of the incident wave to the overall acoustic pressure distribution in the vessel. Therefore, two anti-nodes were formed at the height of about 20 mm and 57 mm of the standing wave. Fig. 9 shows the difference $\Delta Ps$ of the sound pressure amplitude defined as $(P_s(z)|_{x=0} - P_s(z)|_{x=20})$ with respect to $z$ axis. Two peaks are observed approximately at $z$ of 30 and 50 mm. From these results, the sound pressure amplitude took relatively large values on the center axis and at $z$ of 20 – 30 mm and 50 – 60 mm. These areas were considered to be located at pressure anti-nodes of the standing waves. These positions approximately corresponded with the positions at where the acoustic cavitation bubbles were gathered and at where the particle swarm was flocculated. Therefore, these results indicate the reflected waves from the vessel are very important for flocculating the particle swarm and gathering the acoustic cavitation bubbles.

**Figure 8.** The distribution of *Ps* in the vessel.

**Figure 9.** The difference *ΔPs* of the sound pressure amplitude.

### 3.4 The discussion of the acoustic force.

For air bubbles in water, the relation between the resonant frequency $f^*$ and the resonant radius $a^*$ is expressed by $f^*a^* \approx 3$ [m/s] (Mitome 2001). In the present study, the resonant diameter of the bubble was estimated at 296 μm. Fig. 10 shows the histograms of the diameter $D$ (the diameter of the bubbles which occurred in the case of no particles in the vessel) and the diameter $D^*$ (the diameter of the acoustic-cavitation-oriented bubbles adhering to the surface of the particle), respectively. The calculation process of $D^*$ is as follow. (i) The area of the shadow image of the particle and the bubbles adhering to the particle was measured. (ii) The area as described above was subtracted from the area of the particle. The area of the particle was defined as the area of a circle calculated by the Feret minimum diameter. (iii) The equivalent circular diameter was calculated from the difference between above areas.

By using this method, the diameter of the acoustic-cavitation-oriented bubble induced by the cavitation bubbles which were considered adhering surface of the particle (see Fig.2) was calculated. From Fig. 10, the diameter of the acoustic-cavitation-oriented bubble adhering to the particle was smaller than resonant diameter. Leighton (1994) reported that the bubbles with sizes smaller than the resonant size moved up a pressure gradient toward pressure antinodes, and with those larger than resonant size moved down the gradient toward the node. Mitome (2001) reported that the particles moved toward pressure nodes in the standing wave when the density of the particle was larger than that of the liquid phase. By comparing our results to these established theories, the bubble motion, which was gathered to the pressure antinodes, corresponded with the established theory (Leighton 1994). However, the particle motion in this experiment was different from the established theory (Mitome 2001). Therefore, the results obtained in the present study indicate that the acoustic radiation force acting on the particle was smaller than the acoustic force acting on the bubble adhering to the particle.

In addition, the black line in Fig. 10 shows the ratio of the buoyancy force $F_{b.\ bubble}$ acting on the bubble (which were adhering to the particle) to the gravity force $F_{g,\ particle}$ of the particle (average diameter: 307μm). The ratio increased with the cube of the

bubble diameter, because $F_{g,\ particle}$ was constant ($F_{g,\ particle}$: 0.156 μN) and $F_{b.\ bubble}$ increased with bubble volume. It was found out that the effect of the $F_{b.\ bubble}$ acting on the particle motion was negligible, because the ratios were almost less than 0.10 of the cavitation-oriented bubble. Moreover, the reflectivity of the acoustic energy in the water-air system (99.9 %) was much larger than that in the water-polystyrene system (6.3 %) (Nakamura et al. 2011). Since reflection of the sound wave almost did not occur at the polystyrene particles' surface, the sound wave penetrated through them. Therefore, the spatial heterogeneity of the pressure field became large when the sound wave was propagated from the water phase to the bubbles, and the acoustic radiation force acting on the bubbles was much larger than the forces acting on the particles. As a result, it is considered that the bubbles adhering to the particle were significantly affected by the acoustic force, and then the bubbles lead the particle to the pressure anti-node of the standing wave.

**Figure 10.** The histogram of $D$ and $D$*, and the ratio of $F_{g,\ particle}$ to $F_{b.\ bubble}$.

## 5. CONCLUSIONS

In the present study, the interaction between the particle motion and the acoustic cavitation bubble motion was discussed. The motion of particle and that of the acoustic-cavitation-oriented bubble induced by the acoustic cavitation bubbles were captured by high-speed video camera, simultaneously. We confirmed that the acoustic cavitation bubbles were adhering to the particle surface. Then, the acoustic-cavitation-oriented bubble adhering to the particle was located at almost the same direction as the moving direction of the particle. The stationary position of the particle swarm and the gathered position of the acoustic cavitation bubbles corresponded with the pressure anti-node of the standing wave. Moreover, the reflected wave from the vessel is very important for the particle flocculation in the condition of the present study. The particle flocculation was significantly affected by the acoustic force acting on the bubble. From these results, it is considered that the bubbles were affected by the acoustic force, and then the motion of the bubbles interacted with the particle flocculation.

**ACKNOWLEDGEMENTS**

The present study was promoted and financially supported by Category "A" of the Grants-in-Aid for Scientific Research, Japan Society for the Promotion of Science. We thank JSPS for its help in the financial support.

**REFERENCES**

Brotchie, A., Grieser, F., Ashokkumar, M., 2009. Effect of power and frequency on bubble-size distributions in acoustic cavitation. Phys. Rev. Lett., 102, 084302.

King, L. V. 1934. On the acoustic radiation pressure on spheres. Proc. Roy. Soc., 147, 212-240.

Kozuka, T., 2005. Acoustic micromanipulation. J. ASJ, 61, 154-159.

Kozuka, T., Tuziuti, T., Mitome, H., Fukuda, T. 1997. Noncontact micro manipulation using an ultrasonic standing wave field in water. Trans. JSME, Series C, 63, 241-248.

Leighton, T. G., 1994. The Acoustic Bubble. Academic Press.

Mitome, H., 2001. Micro bubble and sonoluminescence. Jpn. J. Appl. Phy., 40, 3484-3487.

Nakamura, Y., Mori, T., Saito, T. 2011. Proc. of The 43rd autumn meeting of SCEJ, 205.

Nakamura, Y., Saito, T., 2011. Particle motion in a kHz-order-ultrasound-irradiated water. Proc. of the 8th Int. Sym. on Cavitation, 109.

Nyborg, W. L. 1967. Radiation pressure on a small rigid sphere. J. Acoust. Soc Am., 42, 947-952.

Takeuchi, M., Abe, H., Yamanouchi, K., 1994. Ultrasonic micromanipulation of small particles in liquid using VHF-range leaky wave transducers. 1994 IEEE Ultrason. Symp. Proc., 907-911.

Woodside, S. M., Bowen, B. D., Piret, J. M., 1997. Measurements of ultrasonic forces for particle–liquid separations. A.I.Ch.E. J., 43, 1727-1736.

Woodside, S. M., Piret, J. M., Gröschl, M., Benes, E., Bowen, B. D., 1998. Acoustic force distribution in resonators for ultrasonic particle separation. A.I.Ch.E. J., 44, 1976-1984.

Yamakoshi, Y., Noguchi, Y., 1998. Micro particle trapping by opposite phases ultrasonic travelling waves. Ultrasonics, 36, 873-878.

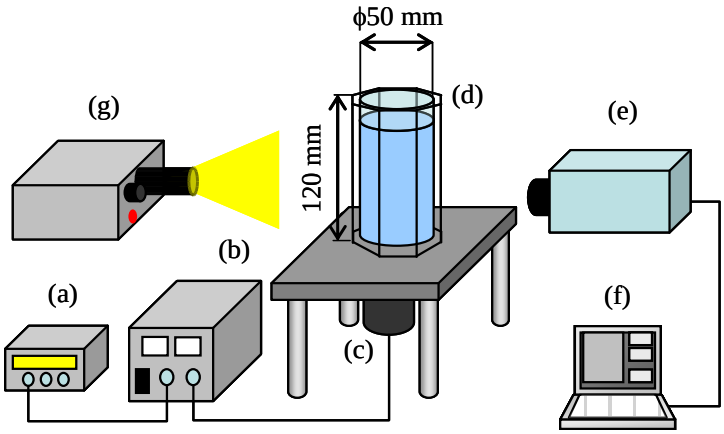


(a) Function generator, (b) Power amplifier, (c) Bolt clamped Langevin type transducer, (d) Acrylic vessel, (e) Camera, (f) PC, (g) Metal halide lamp

**Figure 1.** The schematic of the experimental setup.

**Table 1.** The properties of the particles.

| Material | Polystyrene | | | |
|---|---|---|---|---|
| Density [g/cm$^3$] | 1.05 | | | |
| Average Diameter [μm] | 307 | 396 | 608 | 993 |
| Standard deviation [μm] | 38.9 | 43.2 | 42.6 | 62.1 |

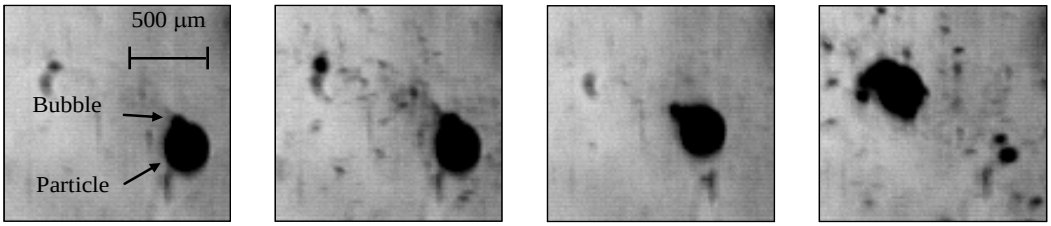


**Figure 2.** Typical snapshots of a particle and the acoustic cavitation bubbles.

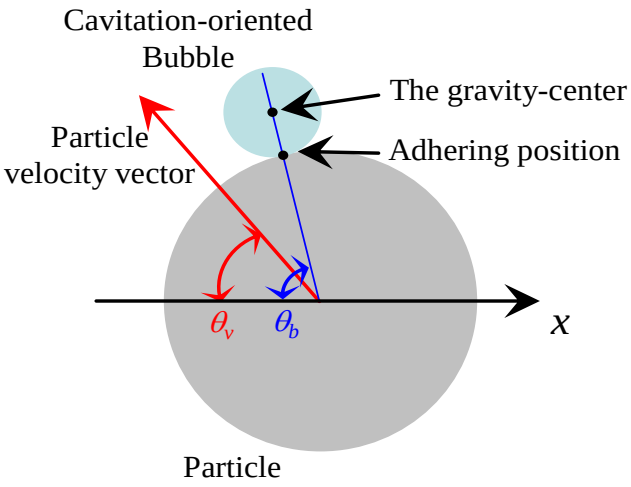


**Figure 3.** The definition of $\theta_v$ and $\theta_b$.

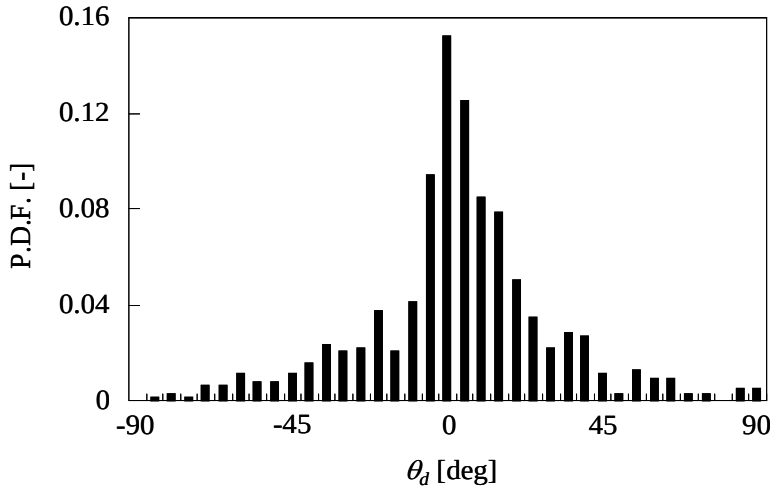


**Figure 4.** The histogram of $\theta_d$.

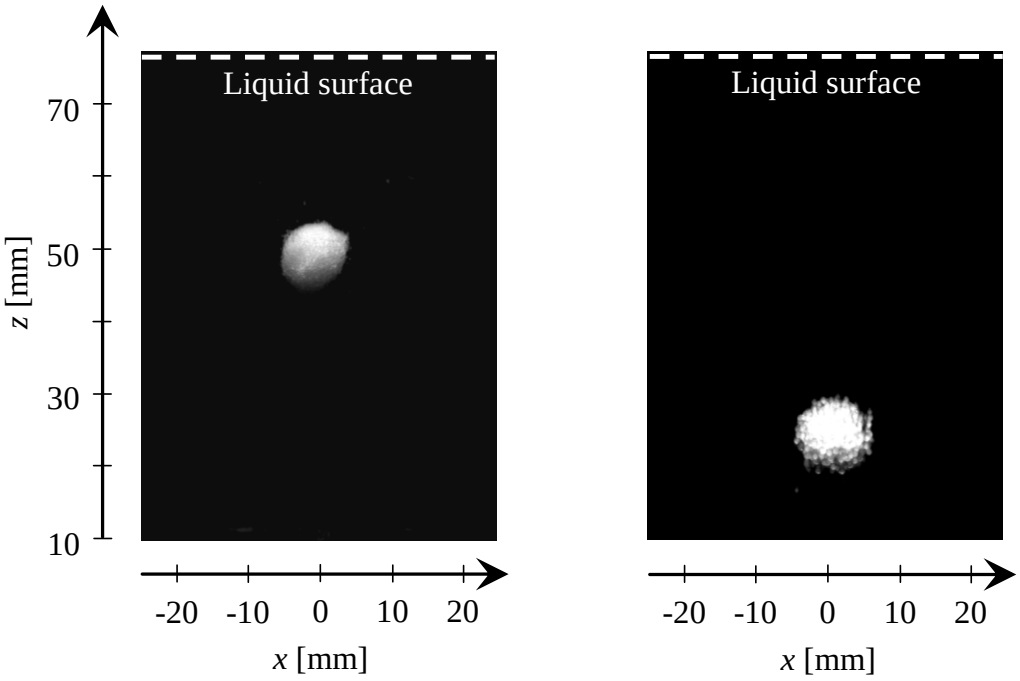


(a) Flocculated particles of 300 μm in average diameter.

(b) Flocculated Particles of 1000 μm in average diameter.

**Figure 5.** Particle swarms in the ultrapure water.

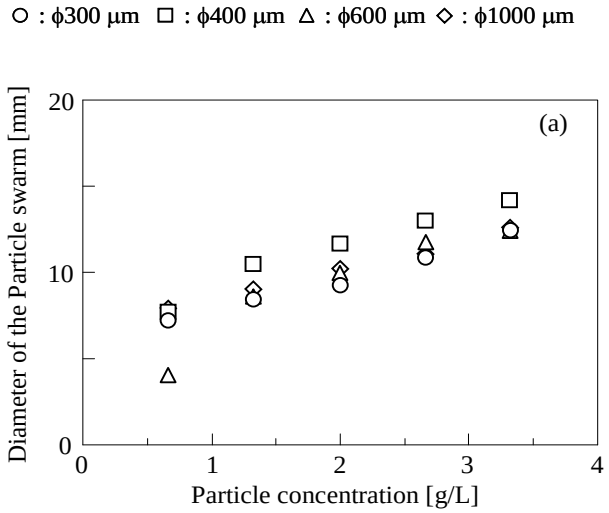


(a) Particle concentration versus a diameter of the particle swarm.

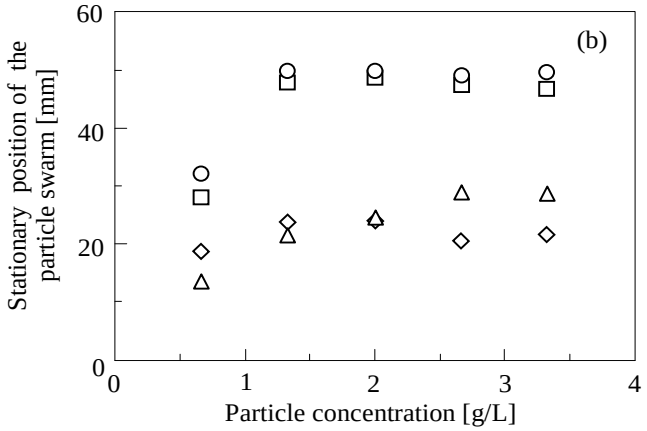


(b) Particle concentration versus a stationary position of the particle swarm.

**Figure 6.** The results of a measurement of the particle swarm.

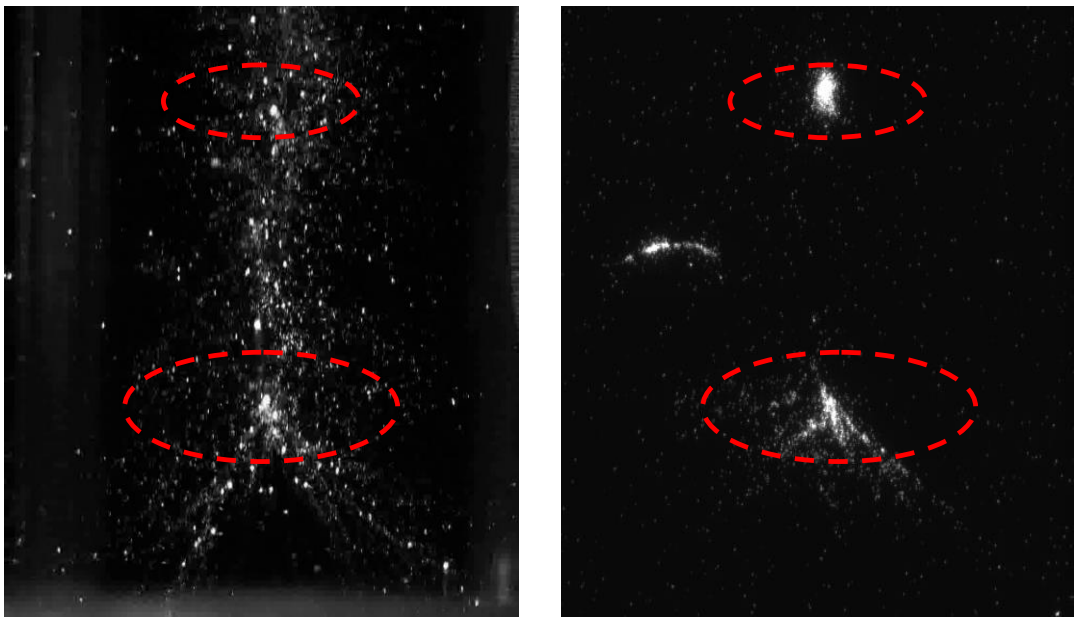

**Figure 7.** The visualization results of the acoustic cavitation bubbles captured by using Laser Tomography (left-side) and the sonoluminescence by using a CCD equipped with an Image Intensifier Unit (right-side).

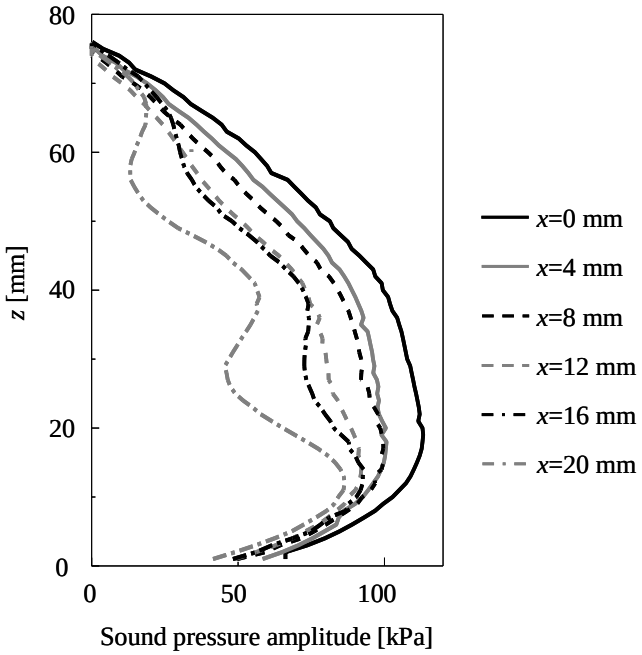


**Figure 8.** The distribution of $P_s$ in the vessel.

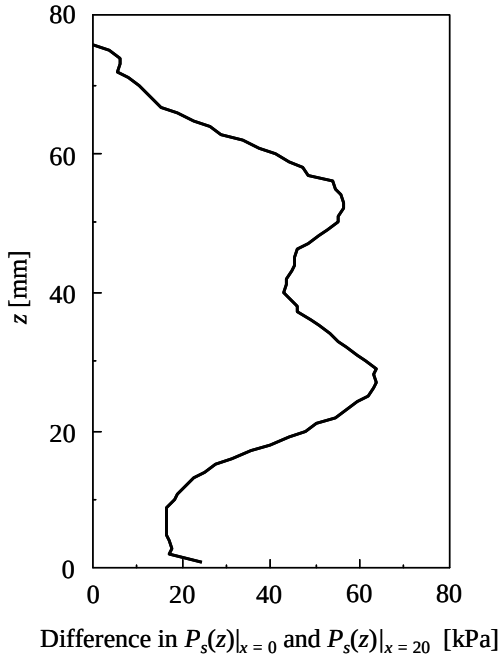


**Figure 9.** The Difference $\Delta P_s$ of the sound pressure amplitude.

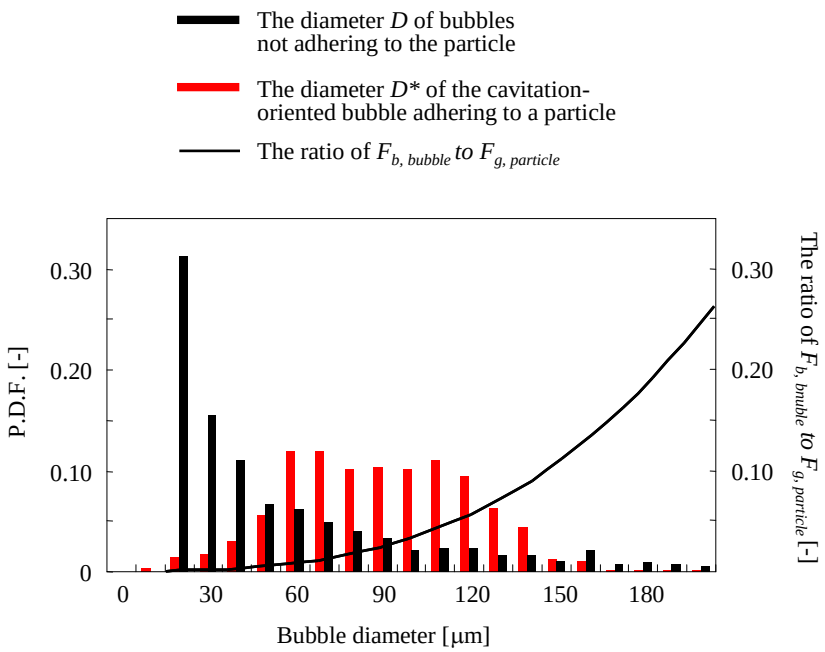


**Figure 10.** The histogram of $D$ and $D^*$, and the ratio of $F_{g,\,particle}$ to $F_{b.\,bubble}$.